Utrecht University

Debye Institute

Nanophotonics Group

Evaporative Cooling in a Bose Gas

Author:
C. Beulenkamp

Supervisors:
Prof. dr. P. van der Straten

June 17, 2015

Abstract

A method of simulating the evaporative cooling of neutral atoms in a magnetic trap is presented. The method is based on kinetic theory and an assumption of ergodicity. An application of this method to the experimental conditions in the Utrecht BEC experiment is compared to measurements. The simulation is found to be accurate down to a temperature of 10 μK. Its predictive power makes it a valuable tool in optimizing the cooling process.

Contents

1 Introduction

Evaporative cooling is the process of cooling through removal of high energy particles. It happens naturally in any system where this removal can take place, such as a hot cup of coffee. The temperature will gradually drop, slowing down the rate of evaporation because the average energy is lowered and less particles are produced that have sufficient energy to escape. Lowering the cutoff energy ensures that evaporation will continue. This is called forced evaporative cooling, and has been crucial in the realization of Bose-Einstein condensation (BEC). It was first demonstrated by Hess et al [5] using atomic hydrogen. The first BEC was made by evaporatively cooling a dilute cloud of rubidium atoms [1]. Cooling to BEC is done by applying radio frequency (RF) induced evaporation to neutral atoms trapped in magnetic traps. The RF radiation flips the spin of the atoms, causing them to be repelled from the trap. The probability of an atom being flipped depends on its height in the potential, and thus its energy.

When probing the properties of Bose-Einstein condensates, a condensate with a large amount of atoms is preferred. To maximize the size of the condensate, the evaporative cooling process has to be optimized. Not much is known about the evolution of the gas, making it difficult to optimize except through trial-and-error. Previous models have been based on the assumption that the distribution has the form of a truncated Boltzmann distribution. This assumption overestimates the rate of evaporation, and is thus not very useful in an experimental setting. In this thesis a model applicable in the lab is given. First, the experimental setup for production of BEC's is described. Kinetic theory then provides a way of calculating the evolution and properties of the gas using only the distribution function. The evaporative cooling process is then simulated. Finally, the simulation is compared to three experiments.

2 Experimental setup and methods

2.1 Experimental setup

A bar of 30 grams of sodium is heated in the oven to roughly 300 °C to create a sodium vapor. Using two diaphragms, a collimated beam of hot atoms is led into a Zeeman slower. The average speed of the atoms at this point is 800 m/s. Along the length of the Zeeman slower are two laser beams, moving in the opposite direction with respect to the atomic beam. The first is resonant to the cycling transition $3^2S_{1/2}, F_g = 2 \rightarrow 3^2P_{3/2}, F_e = 3$. Absorption of photons imparts their momentum to the atoms, slowing them down. As the atoms slow down, the change in the Doppler shift changes the position of the resonance. To ensure maximal absorption a magnetic field gradient is applied along the length of the Zeeman Slower to compensate the Doppler shift using the Zeeman shift. The second beam is a repump beam, resonant to the $3^2S_{1/2}, F_g = 1 \rightarrow 3^2P_{3/2}, F_e = 2$ transition, which ensures no atoms are lost at places where the magnetic field crosses zero.

At the end of the Zeeman slower is the vacuum chamber, where the slowed atoms are caught in a Magneto-Optical Trap (MOT). It consists of three retro-reflected laser beams, a repump beam with a dark spot and a magnetic quadrupole field generated by two anti-Helmholtz coils. The main MOT beams are detuned to slightly below the cycling transition. Atoms that stray from the minimum of the quadrupole magnetic field are more likely to be pushed back by photon absorption. The dark spot in the repump beam decreases the radiation pressure in the center of the trap, allowing for higher densities.

To further increase the phase-space density, the atoms are transferred to the magnetic trap (MT). The trap only confines atoms in the $m_F = -1$ state, so spin-polarization is used to increase the transfer efficiency [15]. After transferring and compressing the cloud, evaporative cooling starts. The RF-field is generated by a single coil antenna with a diameter of 21 mm connected to an amplifier which receives a signal from a synthesizer (Novatech Instruments Inc. DDS8m 100 MHz). To circumvent memory restrictions, the DDS updates the RF-frequency only ten times per second. The clouds are then imaged using absorption imaging or phase contrast imaging.

2.2 Magnetic Trap

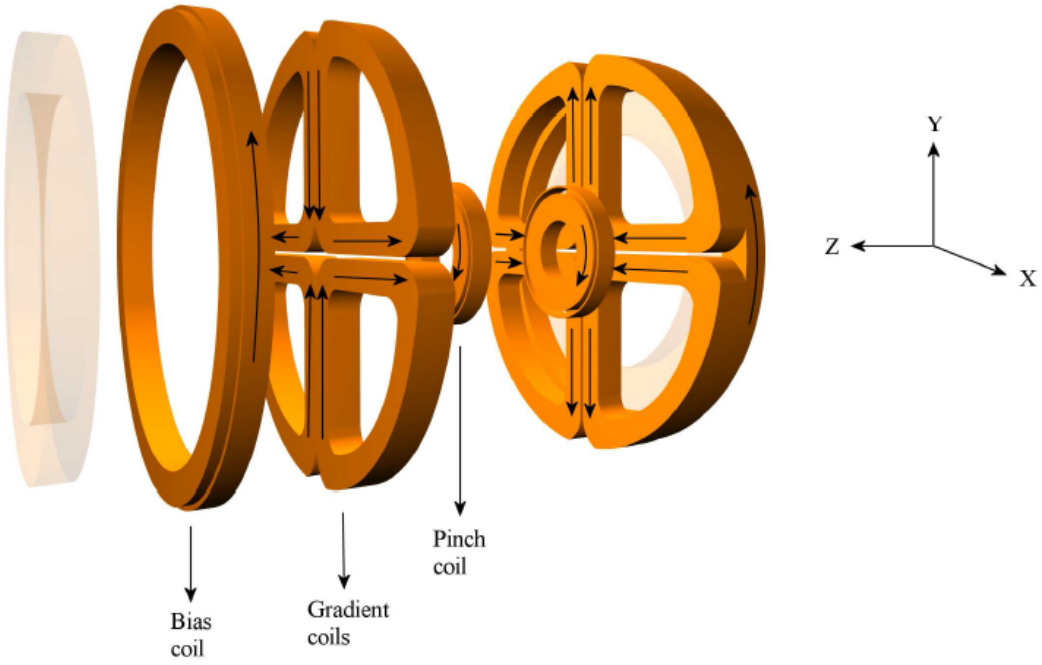

Figure 2.1: A representation of the coils constituting the magnetic trap. [9]
The transparent outer rings are the MOT coils.

The magnetic trap used is an Ioffe-Pritchard type trap in the cloverleaf configuration. The axial trapping is provided by anti-parallel pinch-bias coils and radial trapping by the clover leaves.

In very small magnetic fields, transitions to strong-field seeking states can be induced by the motion of the atoms in the trap. These transitions are called Majorana flops and can cause severe losses due to atoms leaking from the trap at the minimum. To prevent this, the trap has a small bias field B_0.

The potential for an Ioffe-Pritchard trap can be approximated by [7]:

$$U(\mathbf{r}) = g_F \, \mu_\mathrm{B} \, |\mathbf{B}(\mathbf{r})| = \sqrt{\alpha^2(x^2+y^2) + (\beta z^2 + U_0)^2}. \tag{2.1}$$

For energies $\epsilon \ll U_0$ the potential is harmonic:

$$U(\mathbf{r}) = \frac{m}{2}(\omega_\rho^2(x^2+y^2) + \omega_z^2 z^2) + U_0, \tag{2.2}$$

where $\omega_\rho = \frac{\alpha}{\sqrt{mU_0}}$ and $\omega_z = \sqrt{\frac{2\beta}{m}}$.

2.3 Imaging setup

2.3.1 Absorption imaging

A collimated laser beam perpendicular to the z-axis of the trap is led through the cloud . There are two imaging directions with different magnifications. There is top-imaging, which probes from directly above the trap, and side-imaging, which probes at an angle of 45 degrees with respect to the the axis of top-imaging. The atoms are probed at the $F_g = 1$ to $F_e = 1$ transition. To find the fraction of light that has been absorbed, three images are taken: one of the cloud illuminated by the probe beam, one of the probe without atoms and one of the background. The level of absorption is found by subtracting the background from the other two images and then taking their ratio. The signal is then:

$$A(x, y) = e^{-\int \sigma \, \rho(x,y,z) \, dz}, \tag{2.3}$$

where $\sigma = C_{g,e} \frac{3\lambda^2}{2\pi}$ is the absorption cross section with $C_{g,e}$ the relative transition strength from the ground state to the excited state e and ρ is the density distribution of the cloud. After the MT is shut off and the cloud is allowed to expand, the quantization axis is no longer well defined. Assuming that the atoms are randomly distributed over the magnetic sub-levels leads to $C_{g,e} = 5/18$ [8]. During time-of-flight, the cloud expands according to the momentum distribution upon release. When the width due to expansion is larger than the width of the cloud in the trap, a Gaussian distribution can be fitted to the images to estimate the temperature and atom number. In this case, the column density ρ_c is also a Gaussian:

$$\rho_c = \frac{N}{2\pi\sigma_x\sigma_y} e^{-\frac{(x-x_0)^2}{2\sigma_x^2} - \frac{(y-y_0)^2}{2\sigma_y^2}}. \tag{2.4}$$

The atom number N is extracted directly from the images, and the temperature is found by fitting $\sigma(t) = \sqrt{\sigma_0^2 + \frac{k_B T}{m} t^2}$ to a series of images with different time-of-flight.

2.3.2 Phase Contrast Imaging

Phase contrast imaging is based on the phase shift light acquires when it passes through matter. By letting light that passes through the atoms interfere with light that travels around the atoms an intensity profile is created that can be measured by a camera. The advantage of this technique is that the light used for imaging can have a large detuning, keeping absorption low and thus allowing for multiple non-destructive images. This imaging technique was used to measure the trap frequencies, for which only the center of mass has to be determined. More details can be found in [6], [3], [4] and [8].

2.4 Measuring the trap parameters

In order to simulate the cooling process, the trap parameters α, β and U_0 need to be known. The trap frequencies ω_ρ and ω_z and the bottom of the trap U_0 can be measured and used to determine $\alpha = \sqrt{m\omega_\rho^2 U_0}$ and $\beta = \frac{m}{2}\omega_z^2$.

Using phase contrast imaging, the trap frequencies can be determined quickly and accurately. A condensate is prepared in the trap and the minimum is shifted slowly, then rapidly returned to its original position. The resulting oscillation can be fitted to obtain the trap frequencies. Using phase contrast imaging dozens of photos can be made of the same condensate. The speed at which photos can be taken is limited, so several series of photos have to be combined to achieve the resolution to resolve the radial frequency. This measurement combines eight series of fifty photos. The trap frequencies found are $\omega_\rho = 2\pi \times (15.13 \pm 0.03)$Hz and $\omega_z = 2\pi \times (108.01 \pm 0.07)$Hz.

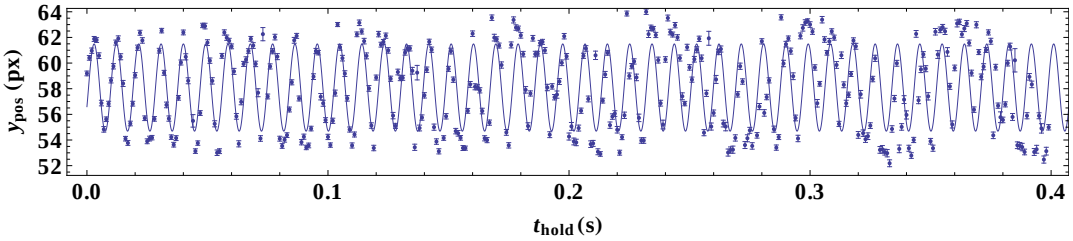

Figure 2.2: Radial oscillation, $R^2 = 0.998494$

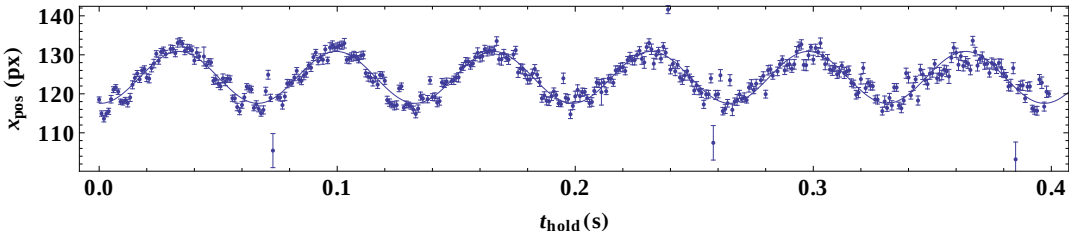

Figure 2.3: Axial oscillation, $R^2 = 0.999697$

The trap bottom U_0 is determined by cooling to BEC and ramping down the RF-frequency. If the ramp goes through the bottom of the trap, all atoms are lost. By scanning the endpoint of the ramp, the trap bottom can be found. For the simulations in this thesis $U_0 = 2\pi\,\hbar \times 2.54$ MHz is used.

3 Theory

3.1 The Boltzmann equation and ergodicity

An ideal gas can be described by a distribution function $f(\mathbf{r},\mathbf{p})$, which is the mean number of atoms at the position $\mathbf{r}$ with momentum $\mathbf{p}$. The evolution of the gas is described by the Boltzmann equation:

$$\left(\frac{\mathbf{p}}{m}\nabla_{\mathbf{r}} - \nabla_{\mathbf{r}}U\cdot\nabla_{\mathbf{p}} + \frac{\partial}{\partial t}\right) f(\mathbf{r},\mathbf{p}) = I(\mathbf{r},\mathbf{p}), \tag{3.1}$$

where I is the collision integral for s-wave collisions in the low energy limit:

$$I(\mathbf{r},\mathbf{p}_4) = \frac{\sigma}{(2\pi\hbar)^3 2\pi m}\int d\mathbf{p}_2 d\Omega'\, q\{f(\mathbf{r},\mathbf{p}_1)f(\mathbf{r},\mathbf{p}_2) - f(\mathbf{r},\mathbf{p}_3)f(\mathbf{r},\mathbf{p}_4)\}. \tag{3.2}$$

with $\mathbf{q} = (\mathbf{p}_3 - \mathbf{p}_4)/2$ the relative momentum and Ω' specifies the direction of the relative momentum after the collision with respect to the relative momentum before the collision. Here $\sigma = 8\pi a^2$ is the collisional cross-section, where $a = 52.98a_0$ [11] is the s-wave scattering length for sodium in the $F_g = 1, m_F = -1$ state. The first term between the brackets describes atoms at position $\mathbf{r}$ with momenta $\mathbf{p}_1$ and $\mathbf{p}_2$ undergoing an elastic collision and having momenta $\mathbf{p}_3$ and $\mathbf{p}_4$ after the collision. The second term describes the opposite process. We will assume "sufficient ergodicity", which means that the distribution of atoms in phase space depends only on their energy:

$$f(\mathbf{r},\mathbf{p}) = \int d\epsilon\, \delta(U(\mathbf{r}) + \frac{p^2}{2m} - \epsilon) f(\epsilon). \tag{3.3}$$

Where $f(\epsilon)$ is the occupation number for a state with energy ϵ and is called the *ergodic distribution function*. The density of states is then given by:

$$\rho(\epsilon) = \int d\mathbf{r}\, d\mathbf{p}\, \delta(U(\mathbf{r}) + \frac{p^2}{2m} - \epsilon). \tag{3.4}$$

Using the assumption of sufficient ergodicity, the Boltzmann equation is reduced to a change in the distribution function $f(\epsilon)$ [7].

$$\begin{aligned}\rho(\epsilon_4)\dot{f}(\epsilon_4) &= \frac{m\,\sigma}{\pi^2\hbar^3}\int d\epsilon_1 d\epsilon_2 d\epsilon_3\, \delta(\epsilon_1+\epsilon_2-\epsilon_3-\epsilon_4)\rho(\min[\epsilon_1,\epsilon_2,\epsilon_3,\epsilon_4])\{f(\epsilon_1)f(\epsilon_2) - f(\epsilon_3)f(\epsilon_4)\} \\ &= \frac{m\,\sigma}{\pi^2\hbar^3}\int d\epsilon_1 d\epsilon_2\, \rho(\min[\epsilon_1,\epsilon_2,\epsilon_1+\epsilon_2-\epsilon_4,\epsilon_4])\{f(\epsilon_1)f(\epsilon_2) - f(\epsilon_1+\epsilon_2-\epsilon_4)f(\epsilon_4)\}\end{aligned}$$

With Bose stimulation included the equation becomes:

$$\begin{aligned}\rho(\epsilon_4)\dot{f}(\epsilon_4) =& \frac{m\,\sigma}{\pi^2\hbar^3}\int d\epsilon_1 d\epsilon_2\, \rho(\min[\epsilon_1,\epsilon_2,\epsilon_1+\epsilon_2-\epsilon_4,\epsilon_4])\times \\ & \{f(\epsilon_1)f(\epsilon_2)(1+f(\epsilon_1+\epsilon_2-\epsilon_4))(1+f(\epsilon_4)) - f(\epsilon_1+\epsilon_2-\epsilon_4)f(\epsilon_4)(1+f(\epsilon_1))[1+f(\epsilon_2))\}\,.\end{aligned}$$

This can be separated into a rate of atoms scattering into a state with energy ϵ_4 and a rate of atoms scattering out of a state with energy ϵ_4.

$$\rho(\epsilon_4)\dot{f}^{\text{in}}(\epsilon_4) = \frac{m\,\sigma}{\pi^2\hbar^3}\int d\epsilon_1\, d\epsilon_2\, \rho(\min[\epsilon_1, \epsilon_2, \epsilon_1+\epsilon_2-\epsilon_4, \epsilon_4])f(\epsilon_1)f(\epsilon_2)(1+f(\epsilon_1+\epsilon_2-\epsilon_4))(1+f(\epsilon_4)) \tag{3.5}$$

$$\rho(\epsilon_4)\dot{f}^{\text{out}}(\epsilon_4) = -\frac{m\,\sigma}{\pi^2\hbar^3}\int d\epsilon_1\, d\epsilon_2\, \rho(\min[\epsilon_1, \epsilon_2, \epsilon_1+\epsilon_4-\epsilon_2, \epsilon_4])f(\epsilon_1+\epsilon_2-\epsilon_4)f(\epsilon_4)(1+f(\epsilon_2))(1+f(\epsilon_1)) \tag{3.6}$$

This second rate describes all elastic collisions for an atom with energy ϵ_4. The average elastic collision rate is thus given by:

$$k_{\text{el}} = \frac{1}{2N}\int d\epsilon\, \rho(\epsilon)\dot{f}^{\text{out}}(\epsilon). \tag{3.7}$$

Where the factor of 2 is due to the double counting of collision events. The collision time is then defined as $\tau_{\text{el}} = k_{\text{el}}^{-1}$.

3.2 Loss processes

During evaporation atoms are lost due to background pressure, dipolar relaxation and three-body recombination, reducing the efficiency of the cooling process. These loss processes are modeled as:

$$\dot{N}_i = -G_i\int d\mathbf{r}\, n^i(\mathbf{r}), \tag{3.8}$$

where i=1,2,3 represent the background pressure, dipolar relaxation and three-body recombination respectively. The loss constants are $G_1 = \frac{1}{\tau}$, with τ the measured lifetime of the atom cloud when held in the MT, roughly 180 seconds, $G_2 = 6\times10^{-17}$ cm^3 s^{-1} [2] and $G_3 = 6.6\times10^{-30}$ cm^6 s^{-1} [13]. These losses can be written in terms of the ergodic distribution function using identity (3.3). Consider the loss due to background pressure:

$$\dot{N}_1 = -G_1\int d\mathbf{r}\, n(\mathbf{r}) = -G_1\int d\mathbf{r}\, d\mathbf{p}\, f(\mathbf{r},\mathbf{p}) = -G_1\int d\mathbf{r}\, d\mathbf{p}\, d\epsilon\, \delta(U(\mathbf{r}) + \frac{p^2}{2m} - \epsilon)f(\epsilon). \tag{3.9}$$

So the change in atom number can be expressed in terms of the change in the distibution function.

$$\dot{N}_1 = \int d\epsilon\, \rho(\epsilon)\, \dot{f}_1(\epsilon) = -\int d\epsilon\, \rho(\epsilon)\, G_1 f(\epsilon) \tag{3.10}$$

The change in the distribution function due to these losses can be written as:

$$\rho(\epsilon)\ \dot{f}_1(\epsilon) = -G_1\,\rho(\epsilon)\,f(\epsilon). \tag{3.11}$$

In a similar way, an expression is found for three-body recombination:

$$\dot{N}_3 = -G_3 \int d^3\mathbf{r}\, n^3(\mathbf{r}) = -G_3 \int d^3\mathbf{r} d^3\mathbf{p}_1 d^3\mathbf{p}_2 d^3\mathbf{p}_3\, f(\mathbf{r},\mathbf{p}_1) f(\mathbf{r},\mathbf{p}_2) f(\mathbf{r},\mathbf{p}_3) \tag{3.12}$$

$$= -G_3 \int d\epsilon_1 d\epsilon_2 d\epsilon_3\, f(\epsilon_1) f(\epsilon_2) f(\epsilon_3) \int d^3\mathbf{r} d^3\mathbf{p}_1 d^3\mathbf{p}_2 d^3\mathbf{p}_3 \prod_{i=1}^{3} \delta(U(\mathbf{r}) + \frac{p_i^2}{2m} - \epsilon_i). \tag{3.13}$$

Where integration over the momentum gives:

$$\int d^3\mathbf{r} d^3\mathbf{p}_1 d^3\mathbf{p}_2 d^3\mathbf{p}_3 \prod_{i=1}^{3} \delta(U(\mathbf{r}) + \frac{p_i^2}{2m} - \epsilon_i) = \left(\frac{2\pi(2m)^{3/2}}{(2\pi\hbar)^3}\right)^3 \int_{U(\mathbf{r}) \leq \min_i \epsilon_i} d^3\mathbf{r}\, (\epsilon - U(\mathbf{r}))^{3/2}, \tag{3.14}$$

which is the three-fold density of states. The i-fold density of states is defined as:

$$\rho_i(\epsilon) = \left(\frac{2\pi(2m)^{3/2}}{(2\pi\hbar)^3}\right)^i \int_{U(\mathbf{r}) \leq \min_i \epsilon_i} d^3\mathbf{r}\, (\epsilon - U(\mathbf{r}))^{i/2}. \tag{3.15}$$

For the Ioffe-Pritchard potential these density of states functions are polynomials. By numerical integration and comparison to the results for a purely harmonic potential, the following polynomials are found.

$$\rho_1(\epsilon) = \rho(\epsilon) = \left(\frac{2\pi(2m)^{3/2}}{(2\pi\hbar)^3}\right) \left(\frac{\pi^2}{4\alpha^2\sqrt{\beta}}\right) (\epsilon^3 + 2U_0\epsilon^2), \tag{3.16}$$

$$\rho_2(\epsilon) = \left(\frac{2\pi(2m)^{3/2}}{(2\pi\hbar)^3}\right)^2 \left(\frac{16\pi}{35\alpha^2\sqrt{\beta}}\right) (\epsilon^{7/2} + \frac{7}{3}U_0\epsilon^{5/2}), \tag{3.17}$$

$$\rho_3(\epsilon) = \left(\frac{2\pi(2m)^{3/2}}{(2\pi\hbar)^3}\right)^3 \left(\frac{3\pi^2}{32\alpha^2\sqrt{\beta}}\right) (\epsilon^4 + \frac{8}{3}U_0\epsilon^3). \tag{3.18}$$

The total loss due to three-body recombination can then be written as:

$$\dot{N}_3 = -G_3 \int d\epsilon_1 d\epsilon_2 d\epsilon_3\, \rho_3(\min_i \epsilon_i)\, f(\epsilon_1) f(\epsilon_2) f(\epsilon_3) = \int d\epsilon_3\, \rho_1(\epsilon_3)\, \dot{f}_3(\epsilon_3). \tag{3.19}$$

So the change in the distribution function is:

$$\rho_1(\epsilon_3)\, \dot{f}_3(\epsilon_3) = -G_3 \int d\epsilon_1 d\epsilon_2\, \rho_3(\min_i \epsilon_i)\, f(\epsilon_1) f(\epsilon_2) f(\epsilon_3). \tag{3.20}$$

And likewise, for dipolar relaxation:

$$\rho_1(\epsilon_2)\, \dot{f}_2(\epsilon_2) = -G_2 \int d\epsilon_1\, \rho_2(\min_i \epsilon_i)\, f(\epsilon_1) f(\epsilon_2). \tag{3.21}$$

3.3 Thermodynamic properties

Given a distribution $f(\epsilon)$, some extensive properties can be calculated. First there are the number of atoms and the total internal energy:

$$N = \int d\epsilon\, \rho(\epsilon)\, f(\epsilon)\,, \qquad U = \int d\epsilon\, \epsilon\, \rho(\epsilon)\, f(\epsilon). \tag{3.22}$$

Then there is the entropy for a system of bosons [10]:

$$\begin{aligned} S &= -k_{\mathrm{B}} \int d^3\mathbf{r} d^3\mathbf{p}\, \{f(\mathbf{r},\mathbf{p}) \log f(\mathbf{r},\mathbf{p}) - (1 + f(\mathbf{r},\mathbf{p})) \log(1 + f(\mathbf{r},\mathbf{p}))\} \\ &= -k_{\mathrm{B}} \int d\epsilon\, \rho(\epsilon) \{f(\epsilon) \log f(\epsilon) - (1 + f(\epsilon)) \log(1 + f(\epsilon))\}. \end{aligned}$$

When $\dot{f}$ is known, the derivatives can also be calculated:

$$\dot{N} = \int d\epsilon\, \frac{\delta N}{\delta f(\epsilon)} \dot{f}(\epsilon) = \int d\epsilon\, \rho(\epsilon)\, \dot{f}(\epsilon)\,, \quad \dot{U} = \int d\epsilon\, \frac{\delta U}{\delta f(\epsilon)} \dot{f}(\epsilon) = \int d\epsilon\, \rho(\epsilon)\, \epsilon\, \dot{f}(\epsilon), \tag{3.23}$$

$$\dot{S} = \int d\epsilon\, \frac{\delta S}{\delta f(\epsilon)} \dot{f}(\epsilon) = k_{\mathrm{B}} \int d\epsilon\, \rho(\epsilon) \log\left[\frac{f(\epsilon) + 1}{f(\epsilon)}\right] \dot{f}(\epsilon). \tag{3.24}$$

Because the gas is not in equilibrium, there is strictly speaking no temperature. However, quasi-temperatures can still be computed which can be useful in describing the gas. In equilibrium, the temperature and chemical potential can be expressed in terms of f and $\dot{f}$. The chemical potential is equal to the change in the Helmholtz free energy $F = U - T\,S$ due to the addition of a particle, where the temperature is constant. Suppose the added atom is put in a state with energy ϵ, i.e. $f(\epsilon) \to f(\epsilon) + \frac{1}{\rho(\epsilon)}$. The corresponding change in F is:

$$\Delta F(\epsilon) = \Delta U(\epsilon) - T\,\Delta S(\epsilon) = \left(\frac{\delta U}{\delta f(\epsilon)} - T \frac{\delta S}{\delta f(\epsilon)}\right) \frac{1}{\rho(\epsilon)} = \epsilon - k_{\mathrm{B}} T \log\left[\frac{1 + f(\epsilon)}{f(\epsilon)}\right]. \tag{3.25}$$

The chemical potential is this change averaged over all accessible states in the system:

$$\mu = \frac{\int d\epsilon \rho(\epsilon)\, \Delta F(\epsilon)}{\int d\epsilon\, \rho(\epsilon)} = \frac{\int d\epsilon \rho(\epsilon)\, (\epsilon - k_{\mathrm{B}}\, T \log\left[\frac{1+f(\epsilon)}{f(\epsilon)}\right])}{\int d\epsilon\, \rho(\epsilon)}. \tag{3.26}$$

This expression can be easily checked by plugging in the Bose-Einstein distribution $f(\epsilon) = (e^{(\epsilon-\mu)/k_{\mathrm{B}}\, T} - 1)^{-1}$. The temperature is defined by:

$$\dot{U} = T\dot{S} + \mu\dot{N}. \tag{3.27}$$

These equations can be used to define a non-equilibrium temperature and chemical potential. Restricting the integration over ϵ to an interval J (where $\dot{N}$, $\dot{U}$, and $\dot{S}$ are also restricted to J) gives local values $\{T(J), \mu(J)\}$.

The temperature defined above is useful for describing the distribution, but is not directly related to experiment. Experimentally, temperature is determined using the free expansion of the cloud. The temperature is thus related to the pressure in the trapped cloud. Consider the pressure tensor [14]:

$$\overleftrightarrow{P}(\mathbf{r}) = \frac{1}{(2\pi\hbar)^3}\int d\mathbf{p}\,\frac{\mathbf{pp}}{m}\,f(\mathbf{r},\mathbf{p}). \tag{3.28}$$

The trace of this tensor gives the scalar pressure:

$$p(\mathbf{r}) = \frac{1}{3}\mathrm{Tr}(\overleftrightarrow{P}(\mathbf{r})) = \frac{1}{3m(2\pi\hbar)^3}\int d\mathbf{p}\,\mathbf{p}^2\,f(\mathbf{r},\mathbf{p}). \tag{3.29}$$

Integrating the scalar pressure over the whole cloud allows a conversion to the ergodic distribution function:

$$\int d\mathbf{r}\,p(\mathbf{r}) = \frac{1}{3m(2\pi\hbar)^3}\int d\mathbf{r}d\mathbf{p}\,\mathbf{p}^2\,f(\mathbf{r},\mathbf{p}) = \frac{1}{3m(2\pi\hbar)^3}\int d\mathbf{r}d\mathbf{p}d\epsilon\,\mathbf{p}^2\,\delta(U(\mathbf{r})+\frac{p^2}{2m}-\epsilon)\,f(\epsilon). \tag{3.30}$$

This leads to expression similar to the densities used to calculate the loss rates:

$$\int d\mathbf{r}\,p(\mathbf{r}) = \int d\epsilon\,\rho_p(\epsilon)\,f(\epsilon), \tag{3.31}$$

where:

$$\rho_p(\epsilon) = \frac{2\pi(2m)^{3/2}}{(2\pi\hbar)^3}\frac{2\pi^2}{32\alpha\sqrt{\beta}}(\epsilon^4+\frac{8}{3}U_0\epsilon^3) \tag{3.32}$$

can be easily found using the result for ρ_3.

The result is an integral of pressure over a volume, so the ideal gas law can be used to define the kinetic temperature:

$$T_k = \frac{\int d\epsilon\,\rho_p(\epsilon)\,f(\epsilon)}{Nk_\mathrm{B}} \tag{3.33}$$

3.4 RF induced evaporation

An RF-field can be used to drive the transition from the $|F = 1, m_F = -1\rangle$ trapped state to the $|F = 1, m_F = 0\rangle$ non-trapped state. The resonance frequency of this transition depends of the Zeeman shift between the two states:

$$\hbar\,\omega_{\mathrm{RF}} = g_{\mathrm{F}}\,\Delta m_{\mathrm{F}}\,\mu_{\mathrm{B}}\,B, \tag{3.34}$$

where $\hbar$ is the reduced Planck's constant, ω_{RF} is the frequency of the applied RF-field, g_{F} is the hyperfine Landé g-factor, m_{F} is the magnetic hyperfine quantum number of the state, μ_{B} is the Bohr magneton and B is the magnetic field strength. The energy $\hbar\,\omega_{\mathrm{RF}}$ is also known as the truncation energy, denoted by ϵ_t, because the distribution function is effectively truncated at this energy due to spin-flipping of atoms that have equal or higher energy. A distinction can be made between evaporation, which is the loss of high-energy atoms through elastic collisions, and spilling, which is atoms with energies just below the truncation energy being lost due to the lowering of the RF-frequency. If the RF-frequency is ramped down too fast, more atoms are lost through spilling and evaporation. If it is ramped down too slowly, atoms are lost to background pressure. The truncation energy can be related to the temperature of the cloud by the truncation parameter $\eta = \frac{\epsilon_t}{k_{\mathrm{B}}\,T}$. This parameter determines the efficiency of evaporation and spilling.

For a given ω_{RF} there is a resonance surface at $\hbar\,\omega_{\mathrm{RF}} = g_{\mathrm{F}}\,\Delta m_{\mathrm{F}}\,\mu_{\mathrm{B}}\,B(\mathbf{r})$ with a width that scales linearly with the amplitude of the RF-field. When the RF power is low, the surface is thin, and there is the possibility of high energy atoms, having higher speeds, passing through the resonance surface before their spin-state is changed. This could lead to inefficient cooling because the most energetic atoms are still trapped. Consider an atom having a speed v moving through a magnetic field gradient $B' = dB/d\rho$ and passing a magnetic resonance with Rabi-coupling $\Omega_{\mathrm{RF}} = \mu_{\mathrm{B}} g_{\mathrm{F}} B_{\mathrm{RF}}/\hbar$. The probability P to make the transition from $m_{\mathrm{F}} = -1$ to $m_{\mathrm{F}} = 0$ is given by [9]:

$$P = 1 - e^{-2\pi\Gamma_{LZ}}. \tag{3.35}$$

Where Γ_{LZ} is the Landau-Zener parameter given by

$$\Gamma_{\mathrm{LZ}} = \frac{\hbar\Omega_{\mathrm{RF}}^2}{4v\mu_{\mathrm{B}} g_{\mathrm{F}} B'}. \tag{3.36}$$

Consider an atom moving only along the radial direction. In the limit $\epsilon \gg U_0$ an atom with an energy $\epsilon > \hbar\omega_{\mathrm{RF}}$ will pass through the surface once in a time $t_{\mathrm{trap}} = \frac{\sqrt{2m\epsilon}}{\alpha}$, which is the time it takes for it to fall to the center of the trap from its highest point in the potential. The magnetic field gradient is approximately $B' = \alpha/\mu_{\mathrm{B}}$.

The amount of atoms of energy ϵ that are left after a time $\Delta\epsilon$ can then be approximated by

$$N_\epsilon(t + \Delta t) = N_\epsilon(t) \times (1 - P)^{\frac{\Delta t}{t_{\mathrm{trap}}}} = N_\epsilon(t) \times e^{-\frac{2\pi\,\Gamma_{\mathrm{LZ}}}{t_{\mathrm{trap}}}\Delta t}. \tag{3.37}$$

It follows that the atoms are removed in a time

$$\tau_{\mathrm{evap}} = \frac{t_{\mathrm{trap}}}{2\pi\,\Gamma_{\mathrm{LZ}}} = \frac{4v\mu_{\mathrm{B}}g_{\mathrm{F}}B'\sqrt{2m\epsilon}}{2\pi\,\alpha\,\hbar\Omega_{\mathrm{RF}}^2} = \frac{4vg_{\mathrm{F}}\sqrt{2m\epsilon}}{2\pi\,\hbar\Omega_{\mathrm{RF}}^2} = \frac{4g_{\mathrm{F}}\sqrt{2m\epsilon}\sqrt{2(\epsilon-\hbar\omega_{\mathrm{RF}})/m}}{2\pi\,\hbar\Omega_{\mathrm{RF}}^2}. \tag{3.38}$$

Due to elastic collisions, the population of atoms having energy ϵ is repopulated in a time of the order of the collision time τ_{el}. The condition for efficient spin-flipping is then $\tau_{\mathrm{evap}} \ll \tau_{\mathrm{el}}$. Incomplete evaporation is most likely at the start of the cooling curve. The temperature is then around 400 μK and the RF-frequency is around 50 MHz. The amplitude of the RF-field is not precisely known but is at least 10 mG [9]. The evaporation times for high energy atoms at the start of the cooling process are plotted in figure 3.1.

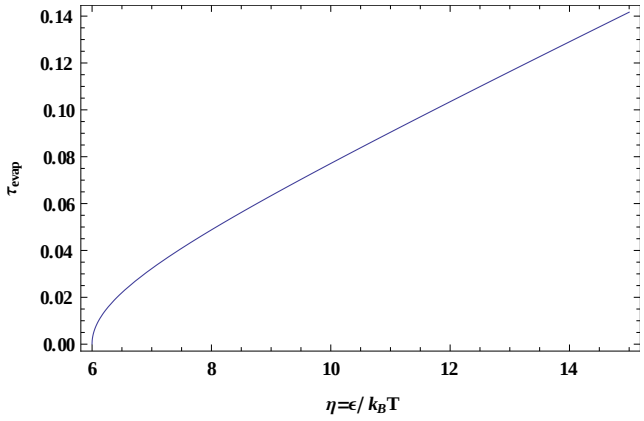

Figure 3.1: Evaporation times for atoms with energy $\epsilon = \eta\, k_B\, 0.0004$.

The average collision rate is roughly 1 s^{-1} , varying slightly with the number of atoms. Because $\tau_{\mathrm{evap}} < \tau_{\mathrm{el}}$, incomplete evaporation can be excluded as having an effect on the cooling process, and the evaporation can be modeled as a complete truncation of the distribution function.

3.5 The shape of a truncated distribution

The Bose-Einstein distribution is the equilibrium distribution because it satisfies *detailed balance*. This means that for any elastic collision involving certain energies $\epsilon_1, \epsilon_2 \rightarrow \epsilon_3, \epsilon_4$, the opposite elastic collision $\epsilon_3, \epsilon_4 \rightarrow \epsilon_1, \epsilon_2$ is equally likely. The truncation of the distribution function breaks the detailed balance between elastic collisions. Collisions producing an atom with $\epsilon > \epsilon_t$ do not have a reverse process. Higher energy particles have a higher chance of these collisions occurring, so the higher energy occupation becomes depleted. Conversely, the lower energy ranges are mostly unaffected. For this reason the distribution can be characterized as being a Bose-Einstein distribution in the limit $\epsilon \rightarrow 0$ and being modified by a correction polynomial for higher energies. The μ and T of the Bose-Einstein distribution are as defined in (3.26) and (3.27), for $J = [0, \epsilon]$ and $\epsilon \rightarrow 0$.

3.6 Effect of gravity on the truncation energy.

Ideally, the surface where the atoms can be spin-flipped and evaporate is an equipotential surface, so that the evaporation depends only on the energy of the atoms. In practice, gravity causes a slight shift between the two. The cloud sags in the magnetic trap due to gravity, so most atoms are lost on the bottom of the evaporation surface. Consider an atom in the center of the trap moving along the direction of gravity. The atom is lost if $\sqrt{\alpha^2\rho_{\rm res}^2 + U_0^2} - U_0 = \epsilon_{t,\rm RF}$. The potential energy is then:

$$\epsilon_t = \epsilon_{t,\rm RF} - m\,g\,\rho_{\rm res} = \epsilon_{t,\rm RF} - m\,g\sqrt{\frac{\epsilon_{t,\rm RF}^2 + 2U_0\,\epsilon_{t,\rm RF}}{\alpha^2}} = \epsilon_{t,\rm RF} + \Delta\epsilon_t, \tag{3.39}$$

where the shift in the minimum $\frac{m}{2}\omega_\rho^2\left(\frac{g}{\omega_\rho^2}\right)^2 = 2\times10^{-3}\,U_0$ is neglected.
Using $\epsilon_t = \eta\,k_{\rm B}\,T$, it follows that:

$$\Delta\eta = \frac{\Delta\epsilon_t}{k_{\rm B}\,T} = -\eta\frac{m\,g}{\alpha}\sqrt{1 + \frac{2U_0}{\eta\,k_{\rm B}\,T}}. \tag{3.40}$$

Below, in figure (3.2), the shift in η is given for different temperature and $\eta = 10$. Note that $\Delta\eta$ does not go to zero at high temperatures due to the linearity of the trapping potential.

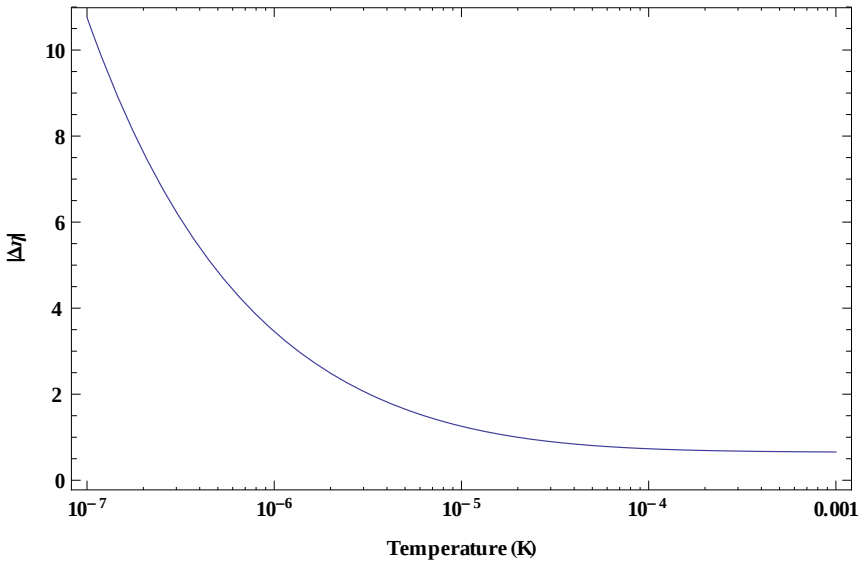

Figure 3.2: $|\Delta\eta|$ for $\eta = 10$.

4 Simulation

4.1 Discretization

In order to simulate the evaporative cooling process, the energy range is divided into bins from 0 to ϵ_t. The resolution is controlled by $n_{\text{bins},k_\text{B}T}$, the number of bins per $k_\text{B}\,T$. The number of bins n_bins is $n_{\text{bins},k_\text{B}\,T} \times \frac{\epsilon_t}{k_\text{B}\,T}$ rounded up. The results presented in this thesis are computed using $n_{\text{bins},k_\text{B}T} = 10$. The bins have width $\Delta\epsilon = \frac{\epsilon_t}{n_\text{bins}}$ and are centered at $\epsilon_i = (i - \frac{1}{2})\Delta\epsilon$. The integrals are approximated using Riemann middle sums.

$$(3.5) \rightarrow \rho_i \dot{f}_i^\text{in} = \frac{m\,\sigma}{\pi^2\hbar^3}\Delta\epsilon^2 \sum_{k=1}^{n_\text{bins}} \sum_{l=\max(i-k+1,1)}^{n_\text{bins}} \rho_{\min[k,l,i,k+l-i]} f_k f_l (1+f_i)(1+f_{k+l-i})$$

$$(3.6) \rightarrow \rho_i \dot{f}_i^\text{out} = \frac{m\,\sigma}{\pi^2\hbar^3}\Delta\epsilon^2 \sum_{j=1}^{n_\text{bins}} \sum_{k=1}^{i+j} \rho_{\min[i,j,k,i+j-k]} f_i f_j (1+f_k)(1+f_{i+j-k})$$

$$(3.11) \rightarrow \rho_i \dot{f}_{1,i} = -G_1 \rho_i f_i$$

$$(3.21) \rightarrow \rho_i \dot{f}_{2,i} = -G_2 \Delta\epsilon \sum_{j=1}^{n_\text{bins}} \rho_2[\min(\epsilon_i, \epsilon_j)] f_i f_j$$

$$(3.20) \rightarrow \rho_i \dot{f}_{3,i} = -G_3\,\Delta\epsilon^2 \sum_{j=1}^{n_\text{bins}} \sum_{k=1}^{n_\text{bins}} \rho_3[\min(\epsilon_i, \epsilon_j, \epsilon_k)] f_i f_j f_k$$

So we have the change in f as a function of f:

$$\dot{f} = y(f) = \dot{f}^\text{in} + \dot{f}^\text{out} + \dot{f}_1 + \dot{f}_2 + \dot{f}_3$$

The μ and T from equations (3.26) and (3.27) can then be computed for any subset with more than one element.

$$T = \frac{1}{k_\text{B}} \frac{\sum_i \rho_i \epsilon_i \dot{f}_i - \frac{\sum_i \rho_i \epsilon_i}{\sum_i \rho_i} \sum_i \rho_i \dot{f}_i}{\sum_i \rho_i \log\left(\frac{f_i+1}{f_i}\right)_i \dot{f}_i - \frac{\sum_i \rho_i \log\left(\frac{f_i+1}{f_i}\right)}{\sum_i \rho_i} \sum_i \rho_i \dot{f}_i} \tag{4.1}$$

$$\mu = \frac{\sum_i \rho_i \epsilon_i}{\sum_i \rho_i} - k_\text{B}\,T \frac{\sum_i \rho_i \log\left(\frac{f_i+1}{f_i}\right)}{\sum_i \rho_i} \tag{4.2}$$

4.2 Method

The DDS used to control the RF-cooling updates the frequency only ten times per second, so the cooling process can be seen as stepwise lowering of the trap depth.When the truncation energy changes, these bins have to be redistributed. To do this for an arbitrary new truncation energy, a continuous distribution is needed. The simulation is divided into chunks of a tenth of a second, which take a distribution and cutoff energy as input and give a best-fit distribution and some other quantities such as the total internal energy, the new atom number and the collision rate as output. Based on the arguments in section 3.5, the fit distribution is of the form:

$$f(\epsilon) = \frac{1}{e^{\beta(\epsilon-\mu)}-1}(1+\sum_{i=2}^{7} p_i\,(\beta\epsilon)^i)\theta(\epsilon_t-\epsilon), \tag{4.3}$$

where $\beta = (k_\mathrm{B}T)^{-1}$ and θ is the Heaviside step function. The evolution of the distribution function is calculated with the Runge-Kutta method. The step-size needs to be small enough to ensure stability of the lowest bin, otherwise the quasi-temperature and quasi-chemical potential cannot be accurately determined. Evaluating the change in f once per collision time of the lowest bin ensures this stability: $\Delta t = \frac{2f_1}{\dot{f}_1^{\mathrm{out}}}$. The distribution at time $t+\Delta t$ is then:

$$f(t+\Delta t) = f(t) + \frac{\Delta t}{6}(k_1+2k_2+3k_3+k_4). \tag{4.4}$$

where:

$$\begin{aligned} k_1 &= y(f)\\ k_2 &= y(f+\frac{\Delta t}{2}k_1),\\ k_3 &= y(f+\frac{\Delta t}{2}k_2),\\ k_4 &= y(f+\Delta t\,k_3). \end{aligned}$$

This process is repeated until 0.1 seconds have passed, at which point the μ and T from equations (3.26) and (3.27) are computed, summing over the first two bins. The distribution (4.3) with these μ and T is then fitted to the f_i. The simulation is written mainly in Mathematica, with a module that computes the change in f during 0.1 seconds. The Riemann sums were written in C, using OpenMP to parallelize the sums, and were made usable by Mathematica using LibraryLink.

5 Experiments

5.1 Linear Ramps

Two linear ramps were measured for comparison with the simulation. Just after loading the MT the precise energy distribution is not well known, due to the high optical density, temperature and because evaporative cooling has already been taking place for a few seconds due to atoms sticking to the windows of the vacuum chamber. A well determined starting point was prepared by ramping the RF-frequency from 60 to 40 MHz in 20 seconds and allowing the cloud to thermalize for 5 seconds. Two linear ramps were examined, one going from 40 to 7 MHz in 30 seconds (figures 5.1 and 5.2), and one going from 40 to 7 MHz in 50 seconds (figures 5.3 and 5.4). Each ramp was sampled at 11 equally spaced points. At each point 6 photos were taken, with a time-of-flight of 10 to 15 milliseconds.

During the experiment the amount of atoms transferred to the MT can fluctuate, so the starting point was measured at the beginning, middle and end. For every section between two reference measurements, the simulation was run with three different starting values: the smallest number of atoms and largest temperature measured (red), the average number of atoms and temperature (blue) and the largest number of atom and lowest temperature (green). The simulation temperatures displayed are the kinetic temperature defined in section 3.3.

The simulations were run with and without the correction for gravity (3.39) to the truncation energy. The correction only applies along the direction of gravity, so neglecting the effect of gravity will underestimate the rate of evaporation and including it will overestimate it. This can be seen by comparing the temperature graphs with and without the compensation for gravity. The simulations without the correction for gravity have a slightly higher temperature than found experimentally and those with the correction have a temperature slightly lower. This implies that there is an effective truncation energy between the two.

5.1.1 30 second ramp

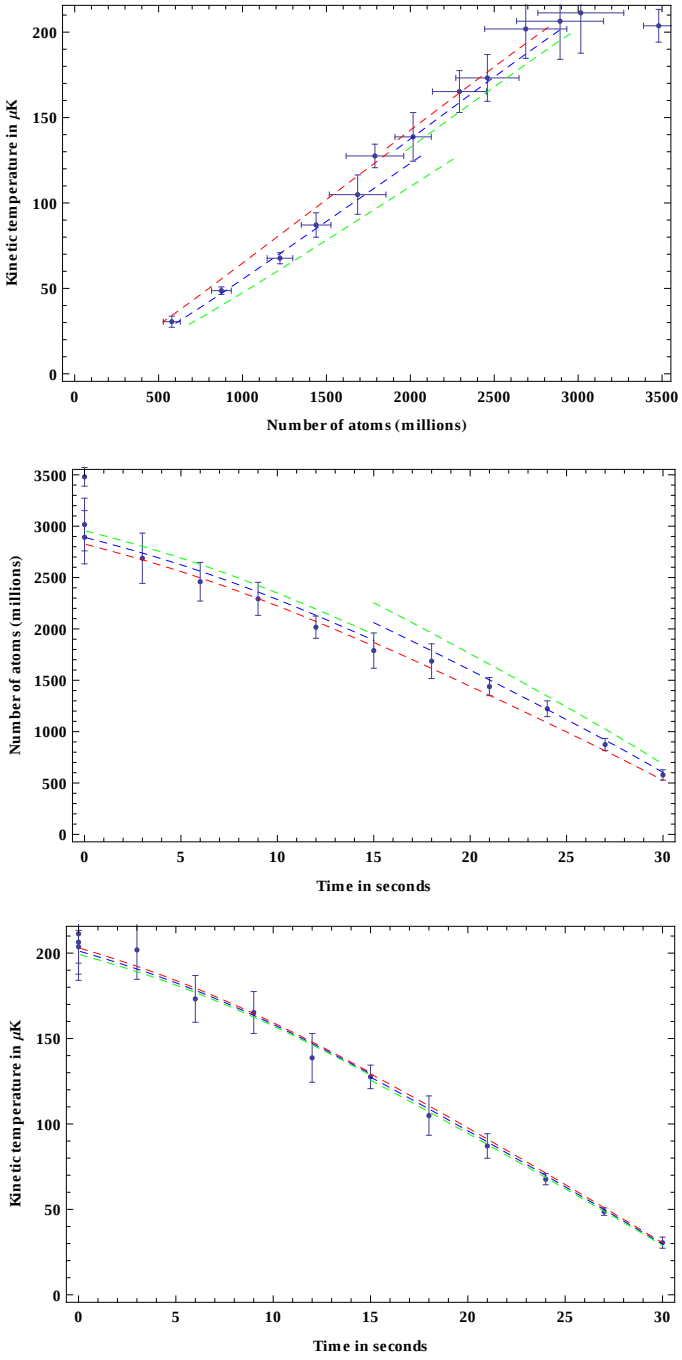

Figure 5.1: Experiment and simulations without adjustment for gravity.

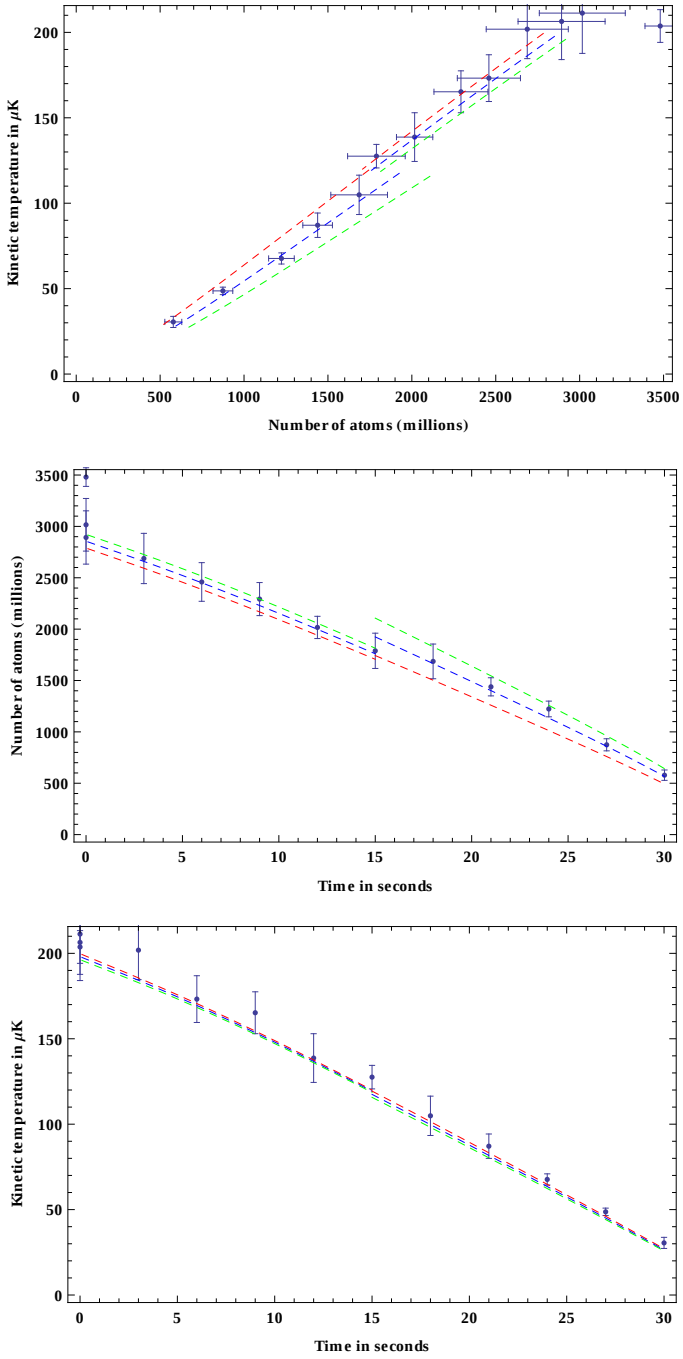

Figure 5.2: Experiment and simulations with adjustment for gravity.

5.1.2 50 second ramp

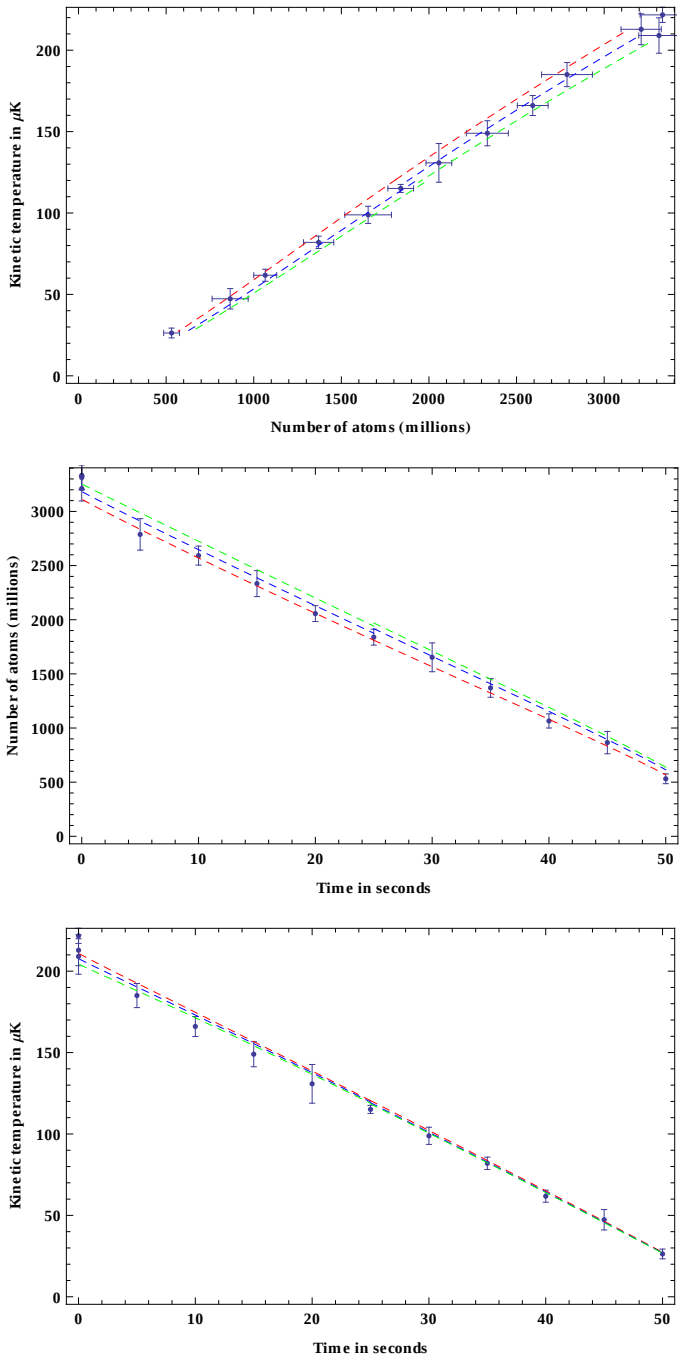

Figure 5.3: Experiment and simulations without adjustment for gravity.

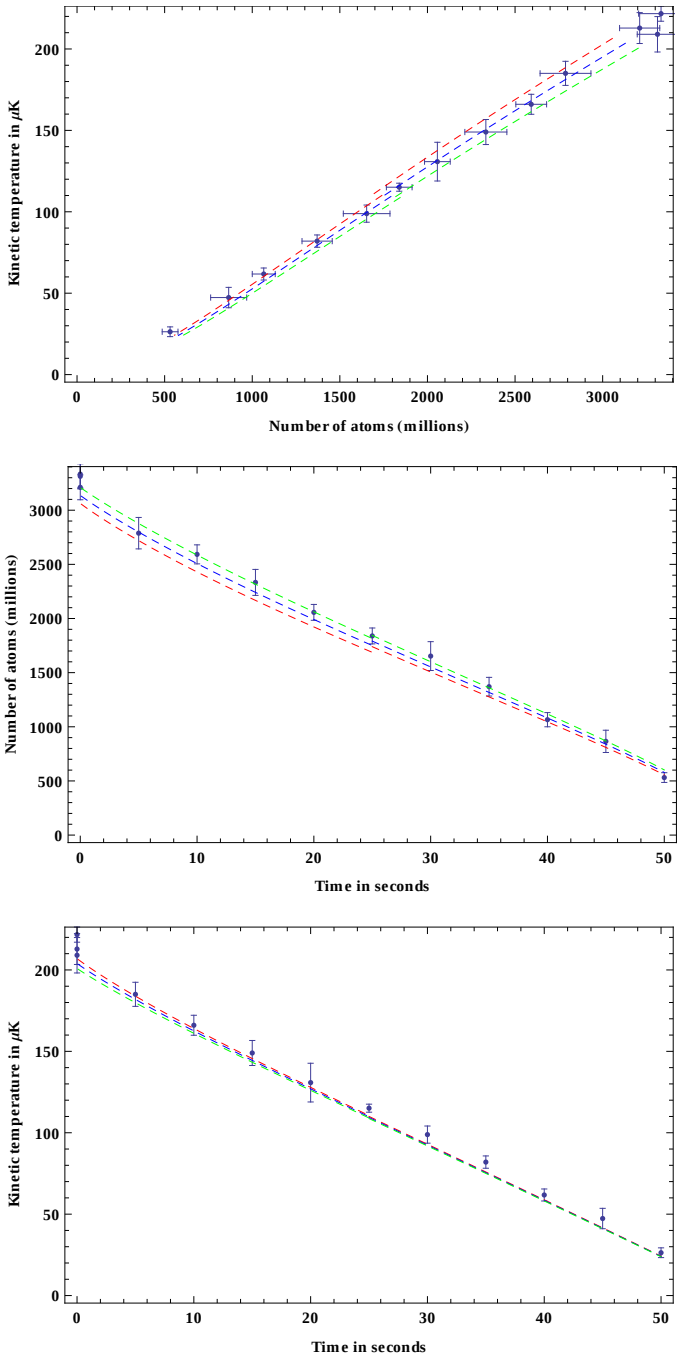

Figure 5.4: Experiment and simulations with adjustment for gravity.

5.2 An optimized path in the harmonic regime

Reaching BEC with a large number of atoms requires that the average energy is reduced while losing as few atoms as possible. Judging the quality of a cooling curve can be done by examining the efficiency parameter:

$$\alpha = -\frac{d\log\left(\frac{U}{N}\right)}{d\log N} = -\frac{\partial_t(U/N)}{U/N}\frac{N}{\partial_t N} \tag{5.1}$$

An optimized path is calculated by maximizing α at each step, lowering the truncation energy until α has passed a maximum. One such path was examined in the harmonic regime, i.e. $\epsilon < U_0$. The reference point for this experiment was when the average particle energy was equal to U_0, which corresponds to a temperature of roughly 40 μK. The simulations are run in the same way as with the linear ramps, using starting values based on the reference measurements before and after. The time-of-flight was increased to 15 - 20 milliseconds, to keep the optical density low enough to extract the atom number from the images. Figure 5.5 shows the data and gravity-corrected simulations for each of the three segments. The atom number and temperature graphs are split into two parts to make all the error bars visible. In between the second and third segment, the power in the laser beams was restored to optimal conditions.

5.2.1 Cooling in the harmonic regime

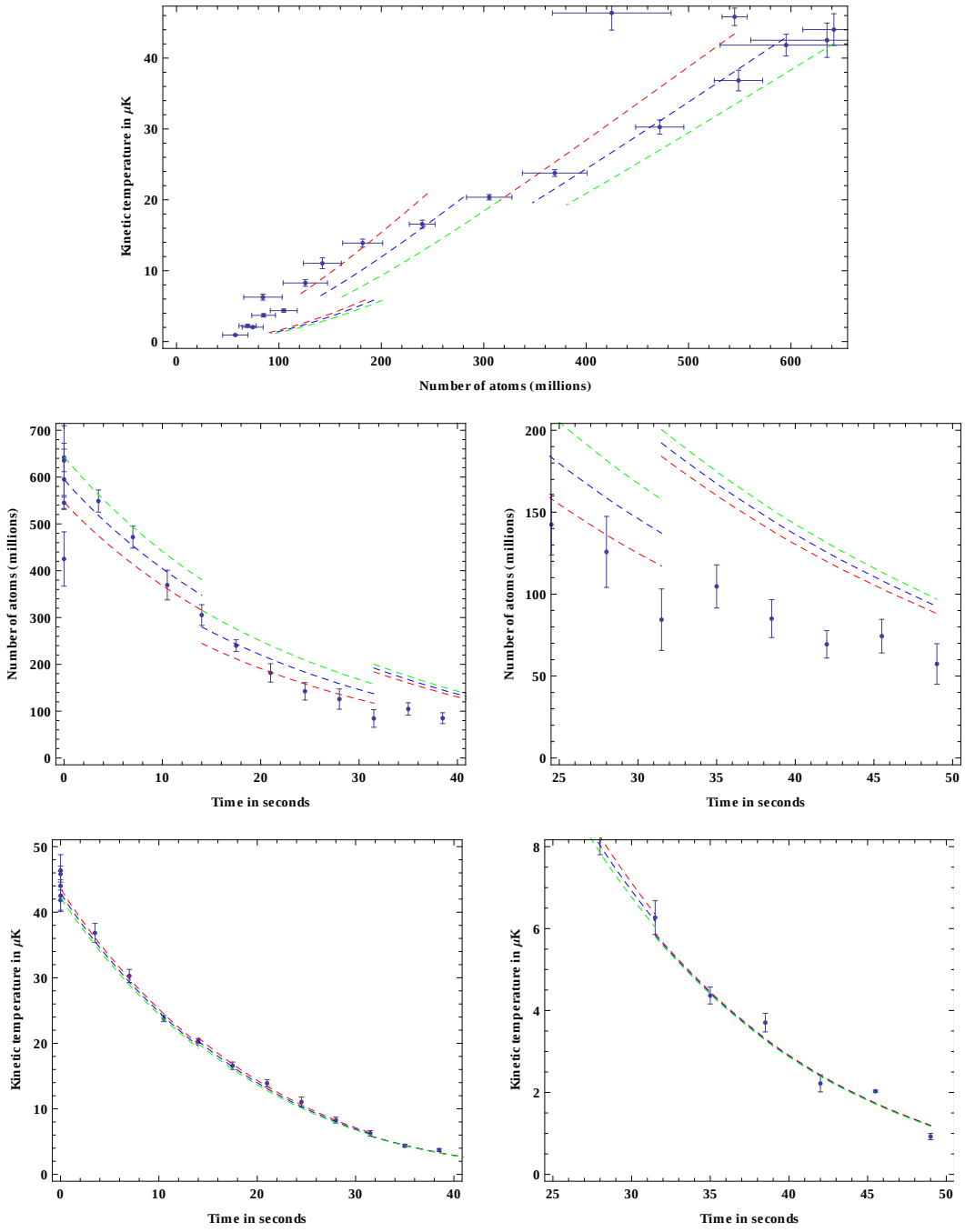

Figure 5.5: Simulation and experiment for the optimized curve.

6 Discussion & Conclusion

The kinetic theory approach accurately predicts the cooling process at higher temperatures, but appears to break down when the gas reaches a temperature of roughly $10\,\mu K$. The reason for this is still unclear. Some possibilities to consider are:

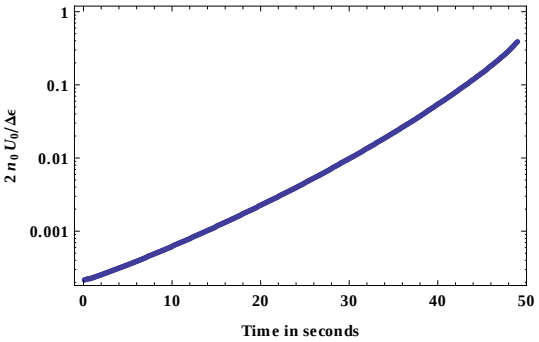

Figure 6.1: Interaction energy

- At high densities loss rates can grow exponentially due to collisional avalanches [12] [16]. This occurs when the collisional opacity κ exceeds 0.693. At the point in the curve where the simulations fails, the collisional opacity is only about 0.03.
- In this model, evaporation occurs directly once an atom with energy $\epsilon > \epsilon_t$ is produced. If the collision rate is larger than the trap frequency, they may collide before evaporating, redistributing their energy. However, at the point where the simulation fails the collision rate for atoms with energy ϵ_t is roughly 6.5 s^{-1}, less than half of the lowest trap frequency.
- The gas is considered to be ideal, but at high densities this is no longer the case. The interaction energy that an atom at the center of the trap has is $2n_0\,U_0^{\text{int}}$, where n_0 is the peak density and $U_0^{\text{int}} = \frac{4\pi\hbar^2 a}{m}$ is the mean field interaction parameter. When this interaction energy is of the order of the binsize $\Delta\epsilon$, the model is no longer valid. The quantity $2n_0\,U_0^{\text{int}}/\Delta\epsilon$ is plotted in figure 6.1. The interaction energy is still less than one-hundredth of the binsize when the experimental data and simulations diverge, so this is likely not the solution.
- The last segment of the cooling curve in the harmonic regime is very unstable. Measuring this curve with the stability achieved in the 50 second linear ramp experiment may give more insightful results, but this will have to be done after this thesis is written. A stable and accurate experiment for cooling below 10 μK can also be used to examine the effective truncation energy due to gravitational sag.

The simulation's accuracy for most of the cooling process indicates it can be a valuable tool in optimizing the production of BEC's. One important improvement to the model would be decompression of the trap. For a sufficiently high initial phase space density, the trap has to be decompressed to decrease losses due to avalanches. A change in the trap parameters will change the energy of an atom according to its position. Incorporating it into the model requires calculating the corresponding change in the distribution function.

7 Acknowledgments

During my year at Nanophotonics I've discovered an urge to figure things out that is stronger than ever before. In particular, I'd like to thank Peter for supervising me and Jasper and Qiao for babysitting me this year. Furthermore, I'd like to thank the ablation master students for letting me hog the big desk, and everyone at Nanophotonics for keeping me company during coffee breaks, lunch, etc.

References

[1] M. H. Anderson, J. R. Ensher, M. R. Matthews, C. E. Wieman, and E. A. Cornell. Observation of Bose-Einstein Condensation in a Dilute Atomic Vapor. *Science*, 269:198–201, July 1995.

[2] H. M. J. M. Boesten, A. J. Moerdijk, and B. J. Verhaar. Dipolar decay in two recent bose-einstein condensation experiments. *Phys. Rev. A*, 54:R29–R32, Jul 1996.

[3] P.C. Bons. *Probing the properties of quantum matter*. PhD thesis, Universiteit Utrecht, 2015.

[4] A. Groot. *Excitations in hydrodynamic ultra-cold Bose gases*. PhD thesis, Universiteit Utrecht, 2015.

[5] Harald F. Hess, Greg P. Kochanski, John M. Doyle, Naoto Masuhara, Daniel Kleppner, and Thomas J. Greytak. Magnetic trapping of spin-polarized atomic hydrogen. *Phys. Rev. Lett.*, 59:672–675, Aug 1987.

[6] S.B. Koller. *Experiments on Hydrodynamic Transport in Ultra-Cold Bose Gases*. PhD thesis, Universiteit Utrecht, 2012.

[7] O. J. Luiten, M. W. Reynolds, and J. T. M. Walraven. Kinetic theory of the evaporative cooling of a trapped gas. *Phys. Rev. A*, 53:381–389, Jan 1996.

[8] R. Meppelink. *Hydrodynamic excitations in a Bose-Einstein condensate*. PhD thesis, Universiteit Utrecht, 2009.

[9] E.D. Ooijen. *Realization and Illumination of Bose-condensed Sodium Atoms*. PhD thesis, Universiteit Utrecht, 2005.

[10] L. E. Reichl. *A modern course in statistical physics*. Arnold, London, 1980.

[11] C. Samuelis, E. Tiesinga, T. Laue, M. Elbs, H. Knöckel, and E. Tiemann. Cold atomic collisions studied by molecular spectroscopy. *Phys. Rev. A*, 63:012710, Dec 2000.

[12] J. Schuster, A. Marte, S. Amtage, B. Sang, G. Rempe, and H. C. W. Beijerinck. Avalanches in a bose-einstein condensate. *Phys. Rev. Lett.*, 87:170404, Oct 2001.

[13] D. M. Stamper-Kurn, M. R. Andrews, A. P. Chikkatur, S. Inouye, H.-J. Miesner, J. Stenger, and W. Ketterle. Optical confinement of a bose-einstein condensate. *Phys. Rev. Lett.*, 80:2027–2030, Mar 1998.

[14] D.G. Swanson. *Plasma Kinetic Theory*. Series in Plasma Physics and Fluid Dynamics. CRC Press, 2008.

[15] K. M. R. van der Stam, A. Kuijk, R. Meppelink, J. M. Vogels, and P. van der Straten. Spin-polarizing cold sodium atoms in a strong magnetic field. *Phys. Rev. A*, 73:063412, Jun 2006.

[16] K. M. R. van der Stam, R. Meppelink, J. M. Vogels, and P. van der Straten. Reaching the hydrodynamic regime in a bose-einstein condensate by suppression of avalanches. *Phys. Rev. A*, 75:031602, Mar 2007.